SAR Analysis
Certification Submission for Medtronic
Percepta CRT-P MRI SureScan / Percepta Quad CRT-P MRI SureScan / Serena CRT-P MRI SureScan / Serena Quad CRT-P MRI SureScan / Solara CRT-P MRI SureScan / Solara Quad CRT-P MRI SureScan / Implantable Devices

(FCC ID: LF5BLEIMPLANT2)

Duane Mateychuk

Eric Zhao, PhD

Wei Gan, PhD

Medtronic, Inc

Mounds View, MN 55112

February 11, 2017

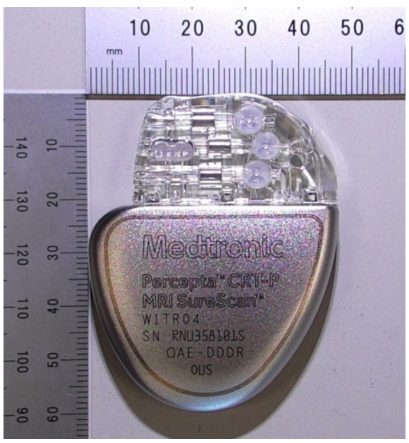

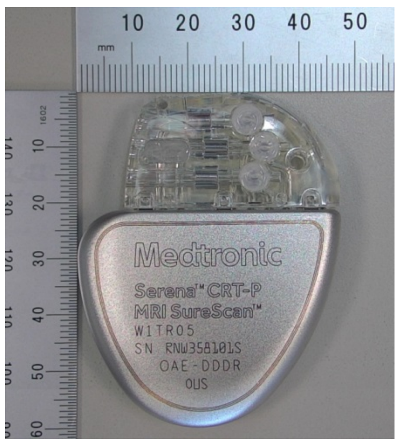

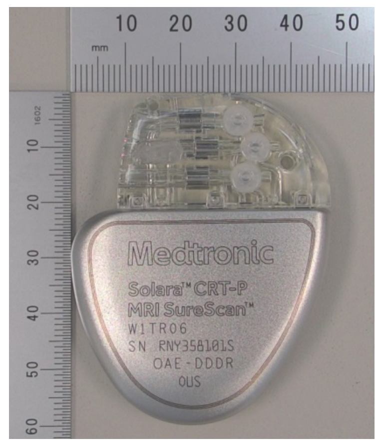

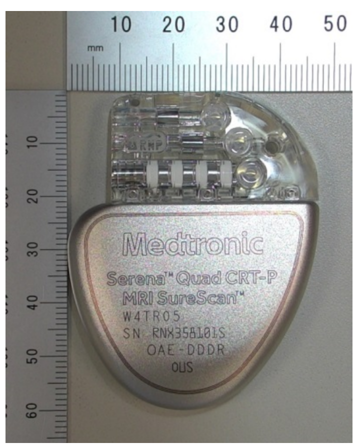

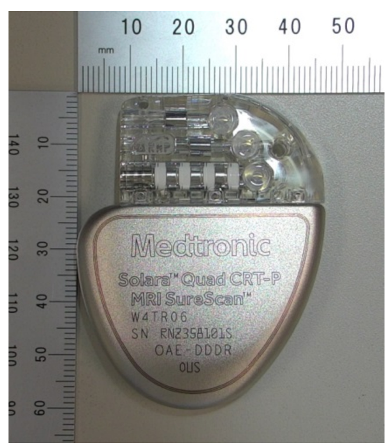

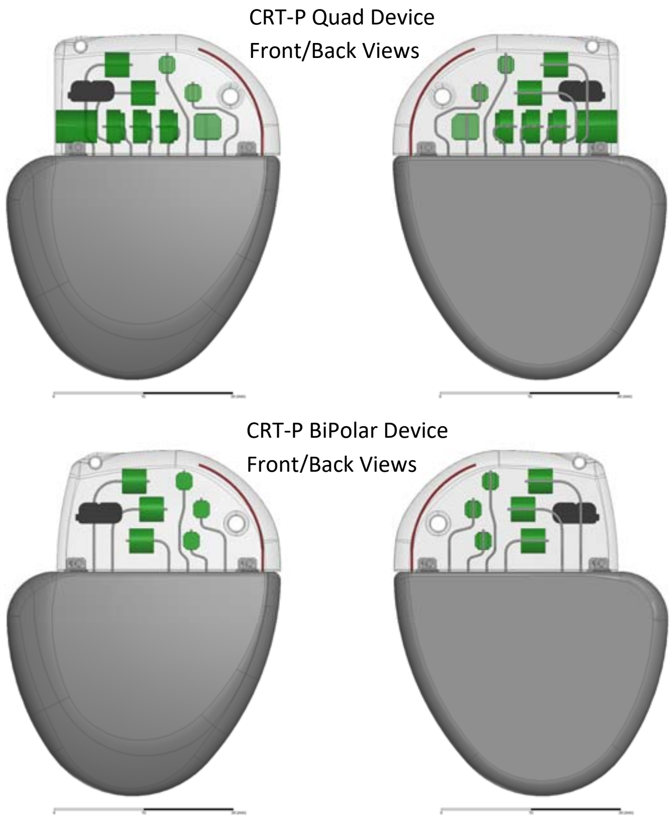

Figure 1: Medtronic Implantable Cardiac Rhythm Disease Management Devices

(Top: Percepta Quad CRT-P MRI SureScan /Serena Quad CRT-P MRI SureScan / Solara Quad CRT-P MRI SureScan Devices front and back views; Bottom: Percepta CRT-P MRI SureScan /Serena CRT-P MRI SureScan / Solara CRT-P MRI SureScan Devices front and back views)

PURPOSE:

This report is a summary of the Finite Element Modeling (FEM) and simulation results of SAR to support the new product certification submittal for the Medtronic CRT-P Quad and CRT-P BiPolar device family (see Figure 1).

Both the CRT-P Quad and CRT-P BiPolar Medtronic implantable devices use Bluetooth Low Energy (BTLE) as the only distance telemetry protocol, and contain the same BTLE transceiver module, which has a fixed RF power output at typically 0 dBm, and up to maximum output at 2.5 dBm, according to the part specifications.

This report satisfies CFR 47, §§1.1307 and §§2.1093, which require radio frequency implanted transmitter manufacturers to show compliance with radio frequency exposure requirements using electromagnetic computational modeling.

METHODOLOGY:

The modeling has taken a conservative approach in assumptions. These assumptions are summarized below:

1. The part has a fixed RF power output of typically 0 dBm at 37°C. Because the device is intended to be implanted in the body, the temperature is well controlled during actual use. RF power output for simulation purposes was set to 2.5 dBm based on the maximum part specification.
2. The maximum RF transmitter output power at the antenna feed-point will be less than the 2.5 dBm power output from the RF transmitter module because of the additional insertion loss in the matching circuit. To be conservative, in this SAR analysis, 2.5 dBm output power is directly applied to the antenna feed-point.
3. Because of the variability of the tissue types and geometry around the device, the tissue that results in the highest SAR was used for this simulation (parallel fiber human muscle).
4. This SAR analysis model uses a 4 cm deep implant location in the human torso model, which allows more transmitted RF power being absorbed by the surrounding tissue instead of radiated into free space, as a worst case for SAR.

The results of the simulations described in this report, based on these conservative assumptions, demonstrate that the spatial peak SAR averaged over 1 gram (cube) of tissue is more than 9 dB below the 1.6 W/Kg General Population/Uncontrolled exposure limit called out in §§2.1093.

HFSS SAR Calculation Process

The computational modeling and simulations within this report were performed with Ansys HFSS™ Finite Element Modeling (FEM) program, part of Ansys Electromagnetics Suite 16.0.

The Specific Absorption Rate (SAR) is a measure of the rate of electromagnetic energy absorbed in a lossy dielectric material. The SAR is a basic scalar field quantity that can be calculated on surfaces or within objects in HFSS. The SAR at a given location is given by the following formula:

$$\mathrm{SAR} = \frac{\sigma_x \cdot |E_x|^2}{\rho_x} + \frac{\sigma_y \cdot |E_y|^2}{\rho_y} + \frac{\sigma_z \cdot |E_z|^2}{\rho_z}$$

where

• σ = the material's conductivity. This is defined as: $\sigma_{bulk} + \omega\varepsilon_0\varepsilon_r tg\delta$

• ρ = the mass density of the dielectric material in mass/unit volume

• E = the RMS electric field in the given location

The method that Ansys HFSS is using to calculate average SAR is described in [1] (Attached appendix to this document).

Medtronic CRT-P Quad and CRT-P BiPolar Devices Numerical Model

The model of the implanted devices is based on the mechanical CAD files which are used to fabricate the actual device components.

As is shown in the Figure 2, the principle of operation for the RF transmission is to drive RF power between the antenna and the welded titanium can which is grounded. Inside device, the RF antenna feed-point is connected to the BTLE module through a matching circuit. Therefore, the maximum RF output power at the antenna feed-point should be always less than the output power from the RF transceiver module because of the additional insertion loss in the matching circuit. Both the CRT-P Quad and CRT-P BiPolar Medtronic implantable devices use Bluetooth Low Energy (BTLE) as the only distance telemetry protocol, and contain the same BTLE transceiver module, which has a fixed RF power output at typically 0 dBm, and up to maximum output at 2.5 dBm, according to the part specifications. **To be conservative, in this SAR analysis, 2.5 dBm (i.e. 1.7783 mW) output power is directly applied to the antenna feed-point.**

The welded titanium can shields any possible RF power emitted directly from the internal electronics, therefore, the internal components do not contribute to the RF radiation as well as SAR. Based on this principle of the operation, the CAD file was simplified and imported into HFSS to create the device model. The simplification is to remove all internal electronic components inside the welded titanium can. The final device model contains all objects outside the device can, such as antenna, header, titanium can, feedthrough, and etc., as seen in Figure 2.

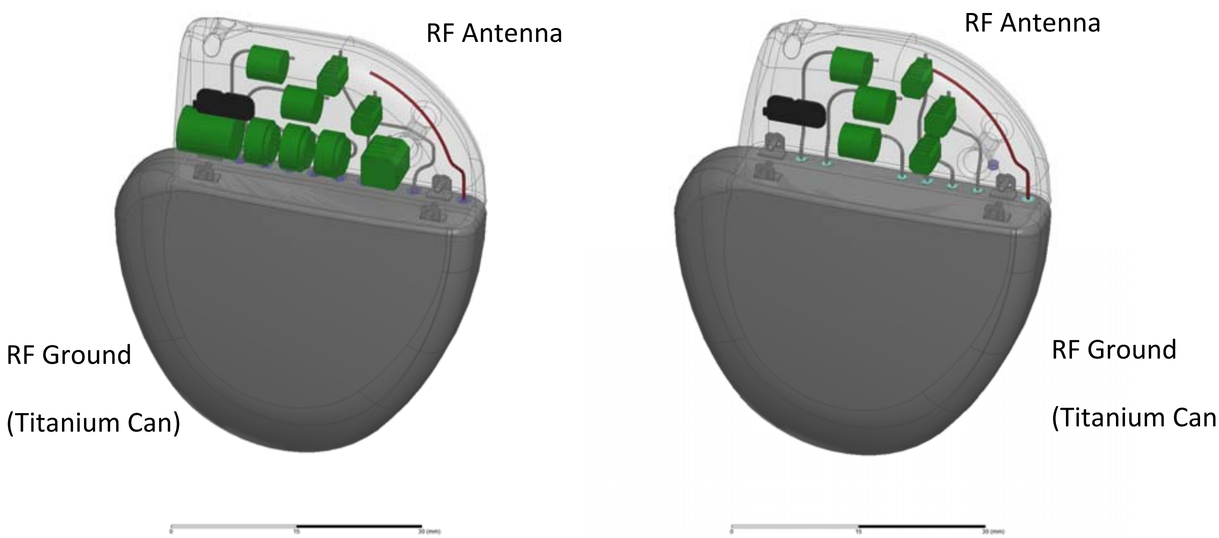

Figure 2: The Implanted Device Model in HFSS (Left: CRT-P Quad and Right: CRT-P BiPolar)

Medtronic CRT-P Device Implant Location and Tissue Properties

The CRT-P devices are typically implanted within the pectoral region of the chest, or implanted in the abdominal area for some patients, and the surrounding tissues may include one or several of the following: muscle, rib, lung, fat, and skin, and the according electrical properties at Bluetooth frequency are listed in Table 1 [2]. Because of this uncertainty of the tissue types and geometry around the device, it is impossible to simulate all implant scenarios. Instead, we should identify the most conservative case, i.e. the implant condition that results in the highest SAR. As can be seen from Table 1, the muscle tissue has higher electrical conductivity than any other types of tissues, which results in more RF power absorption and peak average SAR. Therefore the muscle represents a worst-case scenario for SAR.

Based on this fact, **to be conservative, a human torso model including solely the muscle tissue with the CRT-P implant at the pectoral region was chosen for this model/simulation (Figure 3).** The human torso model is part of the 4 mm resolution full human body model provided by Ansys HFSS. This torso model was used to ensure accurate modeling and to allow reasonable simulation times for determining the spatial peak 1-g average SAR.

Medtronic CRT-P devices are usually located within the pectoral region of the chest at typically 2 cm deep, and up to 4 cm depth. In this SAR analysis model, to be conservative, **the device model is located at 4 cm deep in the human torso model, which allows more transmitted RF power being absorbed by the surrounding tissues instead of radiated into the free space, as a worst case for SAR. This can be also demonstrated by the obvious fact that the antenna radiated power reduces by increased implant depth.**

The location of the implanted device within the human body model is indicated in Figure 3, zoomed-in frontal and side views shown in Figure 4.

	Tissue Type	Relative Dielectric Constant	Conductivity (S/m)
1	Air	1.00	0.00
2	**Human Muscle (parallel fiber, i.e. worst case conductivity)**	**54.38**	**1.90**
3	Human Rib	18.51	0.82
4	Human Lung (inflated)	20.46	0.81
5	Human Lung (deflated)	48.34	1.70
6	Human Fat	5.28	0.11
7	Human Skin (wet)	37.97	1.48
8	Human Skin (dry)	42.81	1.61

Table 1: Electrical Properties (2.48 GHz) of Human Body Tissue at Pectoral Region

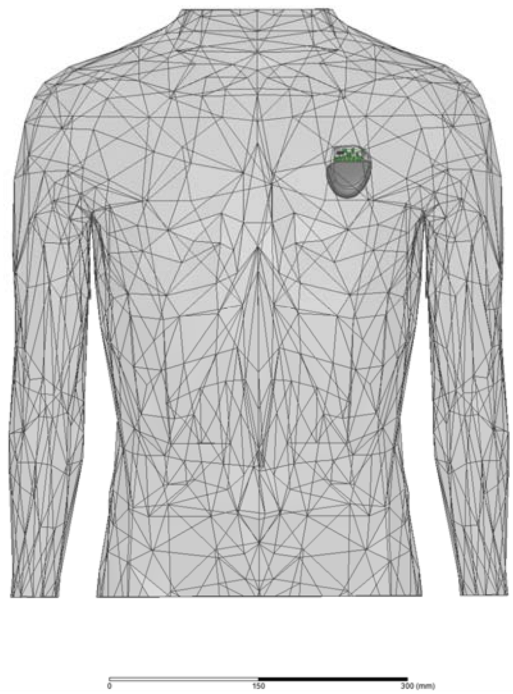

Figure 3: HFSS 4 mm Resolution Human Body Model (with implant shown)

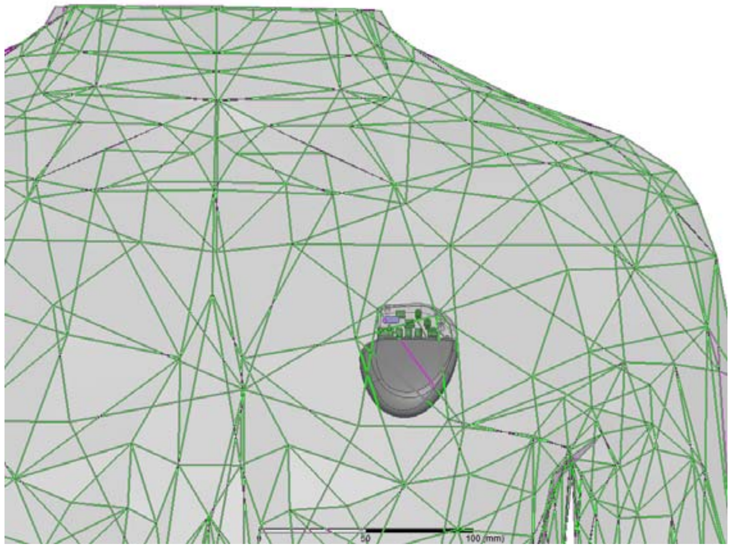

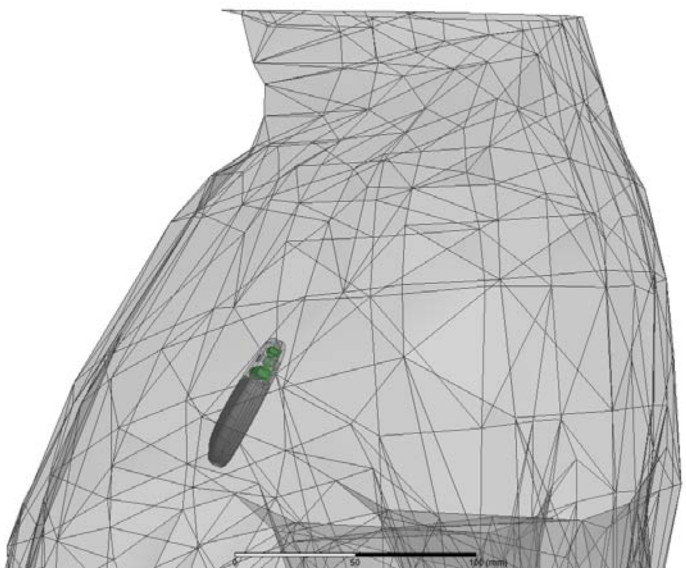

Figure 4: Implanted Device in the Human Body Model

HFSS Human Torso Model for SAR Analysis

An HFSS analysis using the 4 mm, or better, resolution Ansys supplied human body torso model, as illustrated, was used to determine the expected Specific Absorption Rate (SAR) (average in 1 g tissue) when the BTLE transmitter is operated in-vivo. We use the homogenous muscle properties in parallel fiber that represents the worst case electrical conductivity [2]. **The muscle density is specified at 1.06 g/cm^3 in this HFSS model.**

HFSS Meshing Approach and Modeling Parameters

The HFSS software uses the finite element method to discretize the problem space and then calculates the electric and magnetic field vectors at each of the mesh cell vertices. The HFSS mesh resolution uses adaptive refinement which increases mesh resolution in regions with large spatial electric field gradients. The details of this adaptive mesh method can be found in a published paper by Ansys [3].

The human torso model is set in a radiation boundary, which is to simulate an open problem that allows the electromagnetic waves to radiate infinitely far into space.

The program modeling and simulation control parameters are listed below in Table 2.

1)	Solution frequency =2480 MHz (solution frequency for adaptive passes/mesh refinement), which is the highest frequency for BTLE (Channel 39), therefore the worst case scenario concerning the SAR
2)	Maximum number of adaptive passes =15
3)	Maximum refinement per pass =30%
4)	Solution Basis Function = mixed order
5)	Domain Decomposition solver with relative residual 0.0001
6)	Expression Cache of Surrounding Tissue Volume Loss Density field calculator expression with a less than 1% change convergence condition

Table 2: HFSS Modeling/Simulation Control Parameters

HFSS SAR Model Accuracy

The accuracy of the HFSS SAR results is mostly limited by meshing resolution. The error approaches zero if the mesh is dense enough and if the radiation boundary is not too close. To increase the mesh resolution and reduces the mesh induced SAR errors, two enhancements were implemented in the model:

1. A local muscle seed box object surrounding the device model was created to refine the local mesh quality around the surface of the device, where the peak SAR is expected;

2. A second adaptive mesh convergence criteria was added, and the iterations continue until the total integrated energy loss in the local muscle seed box changed by less than 1%.

The modeling accuracy of this SAR analysis is expected to be more than 99% (or less than 1% error) based on the convergence criteria.

The final mesh for the tissue around the device is plotted in Figure 5. As one can see, the highest mesh density is found around the device antenna, where the peak electric field as well as SAR is located.

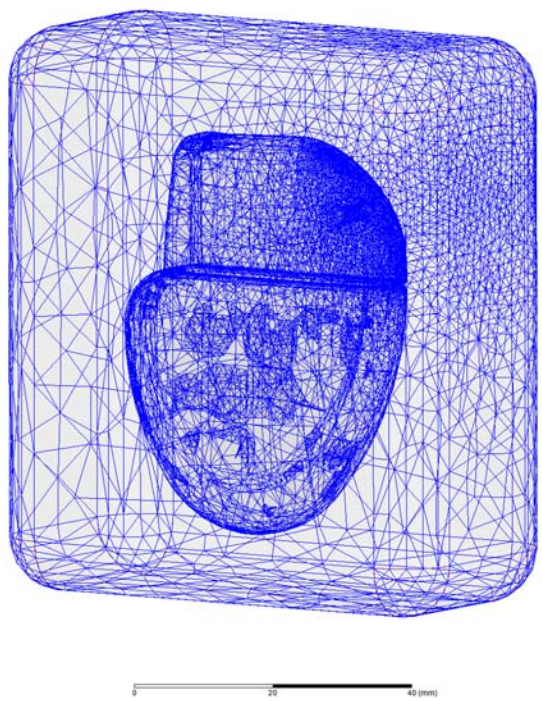

Figure 5: Final mesh plot for the CRT-P Quad SAR Model

HFSS Mesh Statistics
Project: CRTP-QUAD_SAR_Nov15-2016_V0001_1percent_LNX
Design: Truncated_Body
Solution setup: Setup1
Design variation: AirPad='15cm' dFAT='3cm' diaMuscleCylinder='20cm' dSKIN='2mm' dxFAT='1cm' dxFix2='5cm' dxSKIN='2mm' dyPortFix='1mil' dySEED='20mm' dz='0.5897092703mm' dzFAT='5cm' dzFix='19.22893316mm' dzMuscle='3cm' dzSKIN='1mm' hCylinder='20cm' move_y='15mm' move_z='-32mm' Name='14.1335834mm' offsetCyl='20cm' phantom_angle='-25deg' RpadClearance='25mil' zSaline='2cm'

Total number of mesh elements: 2259589

	Num Tets	Min edge length	Max edge length	RMS edge length	Min tet vol	Max tet vol	Mean tet vol	Std Devn (vol)
M957815A001_AF22	104266	0.00809524	0.155809	0.0487091	2.84792e-08	8.42788e-05	6.11114e-06	5.06346e-06
M957814A001_AF32	8535	0.0200904	0.8831	0.277067	1.11921e-07	0.00996931	0.000476084	0.000920797
M960692A001_AF47	6571	0.0218925	0.787583	0.296097	9.09327e-08	0.00223397	6.25744e-05	0.000122784
M960692A001_AF48	182	0.119305	0.889242	0.6198	1.07614e-05	0.00802838	0.00170925	0.00170273
M960692A001_AF49	164	0.223834	0.900425	0.600227	3.68433e-05	0.0137684	0.00190215	0.00207845
M960692A001_AF50	169	0.229918	1.51547	0.63734	1.41749e-05	0.0113578	0.00184458	0.00200761
M960692A001_AF51	170	0.229918	1.66951	0.638153	6.36997e-05	0.00819919	0.00183619	0.00160415
M960692A001_AF52	140	0.243479	0.871633	0.699761	4.75407e-05	0.011032	0.00222829	0.00218389
M960692A001_AF53	143	0.153577	2.3368	0.752849	9.81609e-06	0.0141686	0.00217791	0.00246199
M960692A001_AF54	142	0.228319	1.5604	0.69483	8.40953e-05	0.0116755	0.00219621	0.0018665
M960692A001_AF55	155	0.229918	1.66951	0.665049	5.43029e-05	0.0106797	0.00201004	0.00195977
M183918A006	157	0.344516	2.08094	1.07989	0.000436476	0.142309	0.017346	0.0255124
M183918A006_AF111	557	0.150006	1.54827	0.580503	9.26544e-05	0.0828543	0.00483032	0.00702417
CRTP_FTHRU_INSIDE_BENT_WIRE	776	0.0980426	1.42875	0.563653	2.04914e-08	0.0104315	0.00129534	0.00145894
CRTP_FTHRU_INSIDE_BENT_WIRE_1	690	0.120114	1.30311	0.570718	1.39776e-05	0.0110762	0.00145751	0.00145709
CRTP_FTHRU_INSIDE_BENT_WIRE_2	689	0.143996	1.42875	0.59646	1.19404e-05	0.0150964	0.00146014	0.00165406
CRTP_FTHRU_INSIDE_BENT_WIRE_3	538	0.119305	1.54577	0.68031	1.44311e-05	0.0105791	0.00186687	0.00190322
CRTP_FTHRU_INSIDE_BENT_WIRE_4	505	0.120114	1.75151	0.718675	1.14461e-05	0.0116628	0.00199983	0.00214497
CRTP_FTHRU_INSIDE_BENT_WIRE_5	524	0.181429	2.40142	0.715779	2.44978e-06	0.0168786	0.00191923	0.00236152
CRTP_FTHRU_INSIDE_BENT_WIRE_6	621	0.123548	1.68062	0.639951	1.9797e-05	0.0109095	0.0016172	0.00165288
CRTP_FTHRU_INSIDE_BENT_WIRE_7	604	0.176444	1.25038	0.604928	3.23301e-05	0.00943541	0.00166644	0.00154522
CRTP_FTHRU_INSIDE_BENT_WIRE_8	4177	0.0595296	0.855388	0.33202	1.81411e-07	0.00490468	0.000241664	0.000273842
M958527A_CRTP	767	0.113803	0.991197	0.504129	8.41576e-06	0.00703619	0.00147311	0.00119254
M960095A_LVTIP_FRMD_WIRE	542	0.121217	1.07049	0.474966	4.33145e-05	0.0135831	0.00157722	0.00202934
M960095A_ATIP_FRMD_WIRE	936	0.115311	2.6416	0.793108	1.43009e-05	0.0319548	0.00216855	0.00311621
M960095A_LVR1_FRMD_WIRE	1228	0.121414	0.959703	0.460962	3.95762e-06	0.00849242	0.000873764	0.000944975
M960095A_LVR2_FRMD_WIRE	1105	0.132599	1.24732	0.469339	3.1014e-06	0.0103529	0.00088292	0.00110138
M960095A_LVR3_FRMD_WIRE	1069	0.150739	1.0549	0.46612	2.26272e-05	0.0115975	0.000959436	0.00118575
M960095A_RVRING_FRMD_WIRE	1263	0.130747	2.91159	0.731635	1.47972e-05	0.0218386	0.00187661	0.0026287
M960095A_ARING_FRMD_WIRE	836	0.17706	4.71245	1.11616	1.72928e-05	0.0372066	0.00298695	0.00460747
M183918A006_1	142	0.349379	3.048	1.21598	0.000341257	0.208443	0.019198	0.0284327
M183918A006_2	238	0.389066	2.08864	0.833205	0.0012506	0.142836	0.0114517	0.0134099
M958697A001_17NOV14	325873	0.00401441	3.64929	0.474636	3.78687e-09	0.111821	0.00231686	0.00363887
CBLOCK_170790001	314	0.207083	3.12564	1.78832	2.89648e-05	0.826318	0.102293	0.139608
CBLOCK_170790001_1	664	0.0876162	2.38576	1.19413	2.20033e-06	0.642995	0.0483765	0.0778919
M959728A	1058	0.181912	3.58837	1.61748	0.000161408	2.45509	0.0897449	0.179609
M959730A_SIMPLE	650095	0.0162163	6.9088	0.45542	2.05891e-07	8.55442	0.00782133	0.0758338
M938116A002	234	0.608635	3.55515	2.12328	0.000255363	1.58692	0.292912	0.338286
M938116A002_1	195	0.324253	3.79242	2.51491	2.47079e-05	2.42654	0.351503	0.455262
M938116A002_2	195	0.42572	4.68322	2.65837	0.000113052	3.81384	0.351861	0.562988
M945930A002	89	2.63269	6.9088	4.11879	0.35273	7.62082	1.86789	1.32278
CONTAC_1493410011	88	1.8358	4.23737	3.18906	0.0109229	4.32366	0.612992	0.633269
CONTAC_1493410011_1	76	1.05053	4.99728	3.82637	0.00018719	6.95549	0.711499	0.97838
M959727A	136	0.150065	4.17103	1.96356	1.3719e-05	0.324289	0.0379214	0.0685784
PIN_170784	339	0.284114	1.24014	0.767849	7.43432e-05	0.0399383	0.00593171	0.00686313
PIN_170784_1	339	0.314817	1.24014	0.765055	0.000466329	0.0424774	0.00595106	0.0063386
PIN_170784_2	331	0.345633	1.0668	0.705136	0.000466329	0.034365	0.00608024	0.00571538
PIN_170784_3	454	0.291026	1.0668	0.639818	0.000354748	0.0238961	0.00442552	0.00405386
M957814A001_AF32_3	541	0.141952	2.4955	1.05314	4.29932e-05	0.173303	0.0151081	0.0218636
M957814A001_AF32_3_1	562	0.174971	2.49085	1.02883	3.97674e-05	0.189419	0.0145485	0.0237823
M957814A001_AF32_3_2	487	0.283389	2.4955	1.0524	4.35951e-05	0.159328	0.0167788	0.0221089
M957814A001_AF32_3_3	536	0.224531	2.49085	1.01213	5.71193e-05	0.123569	0.0152626	0.0196867
M957814A001_AF32_3_4	506	0.272625	2.37166	1.04078	4.31695e-05	0.150058	0.0161657	0.0232382
M957814A001_AF32_3_5	539	0.345719	2.3368	1.07192	4.31695e-05	0.313412	0.0151923	0.0242799
M957814A001_AF32_3_6	509	0.232758	2.413	1.01346	3.97674e-05	0.190741	0.0160717	0.0231874
M957814A001_AF32_3_7	483	0.232758	2.4955	1.11163	2.08032e-05	0.149722	0.0169383	0.0222054
M959730A_SIMPLE_10	28919	0.0238754	0.118103	0.0555652	7.45276e-07	4.32602e-05	8.62255e-06	4.95753e-06
Solder_RF_Pin	1252	0.0667724	0.48815	0.184875	2.46251e-06	0.00204631	0.000122696	0.000133307
Can_SolidWorks_Top	18099	0.0130794	8.97246	1.55458	4.41645e-08	1.742	0.0294365	0.0637241
AirCan_SolidWorks	264386	0.0103855	6.3269	0.823197	5.59604e-08	5.95167	0.0438243	0.177245
Can_SolidWorks_Bottom	13017	0.0376425	11.0986	1.67503	3.05492e-07	3.93	0.0437166	0.147081
M959730A_SIMPLE_6	157	0.209402	0.521319	0.37783	0.000167152	0.00443583	0.00158714	0.000886709
M959730A_SIMPLE_9	382	0.153655	0.44343	0.25804	0.000114093	0.00220004	0.000649499	0.00029161
M959730A_SIMPLE_2	94	0.330118	0.545451	0.449147	0.000412099	0.00680226	0.00264258	0.00163261
M959730A_SIMPLE_8	124	0.297376	0.559461	0.408825	2.1014e-05	0.00704501	0.00199628	0.00133671
M959730A_SIMPLE_4	74	0.330118	0.559461	0.480459	0.000698406	0.00696124	0.00335439	0.00179275
M959730A_SIMPLE_5	99	0.285765	0.567286	0.45518	0.00023077	0.00680226	0.00249963	0.00149302
M959730A_SIMPLE_7	90	0.330118	0.545451	0.468215	0.000229594	0.00753553	0.00275016	0.00184156
M959730A_SIMPLE_3	90	0.330118	0.559461	0.447612	0.00045904	0.00667399	0.0027611	0.00170257
M958527A_CRTP_ObjectFromFace1	245	0.150954	0.757154	0.414229	9.11311e-06	0.00592059	0.000981692	0.00106087
GND_Solder	521	0.130544	0.490572	0.255287	1.03351e-05	0.00171496	0.000305257	0.000224311
M960095A_RVTIP_FRMD_WIRE1	1371	0.152382	1.11974	0.572436	2.8887e-05	0.0119809	0.00155338	0.00160335
Region	26929	53.4797	145.239	107.396	7973.33	218946	65745	25099.4
CRTP_NEW_ANT_FORMED1	19491	0.0294339	0.803542	0.269769	3.06257e-07	0.00133533	0.000130976	0.000133536
seed_box	433353	0.0831364	18.9891	1.69772	3.63847e-07	286.296	0.462485	3.86685
air_volume	38285	2.85677	155.462	53.1317	0.149295	205424	9753.17	21886.9
body_exterior	289365	0.958039	22.2846	13.4046	0.048235	613.911	143.809	99.7361

Table 3: Mesh Statistics Summary in CRT-P Quad SAR Model

Table 3 shows the mesh size summary. It shows that there are totally 2,259,589 mesh elements for this SAR model. In the muscle seed box, which is a rectangular tissue volume shown in Figure 5, there are totally 433,353 mesh elements, and the minimum mesh edge size in the volume the device is only 0.0831364 mm. Please note that the edge size of a 1-g muscle cube is about 10 mm, which is about 125 times of the minimum mesh edge size in this model. This high resolution of mesh is resulted from the 1% convergence criteria.

RESULTS:

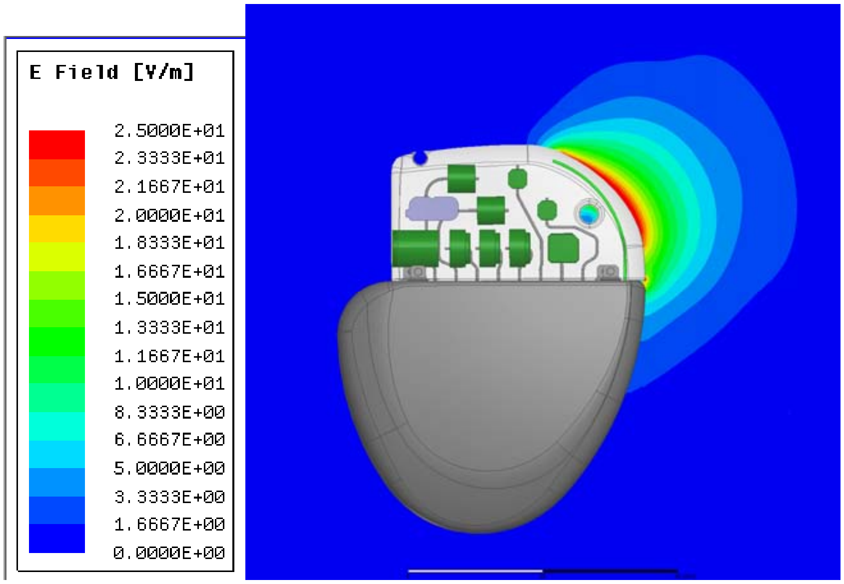

Figure 6: Zoom-In of HFSS simulated electric field in human body model cross-section with Implanted CRT-P Quad Device shown

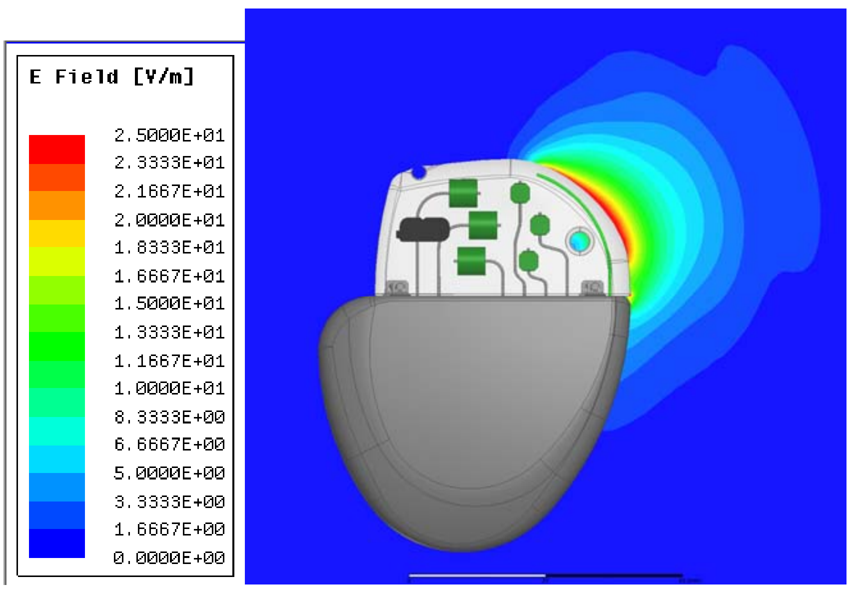

Figure 7: Zoom-In of HFSS simulated electric field in human body model cross-section with Implanted CRT-P BiPolar Device shown

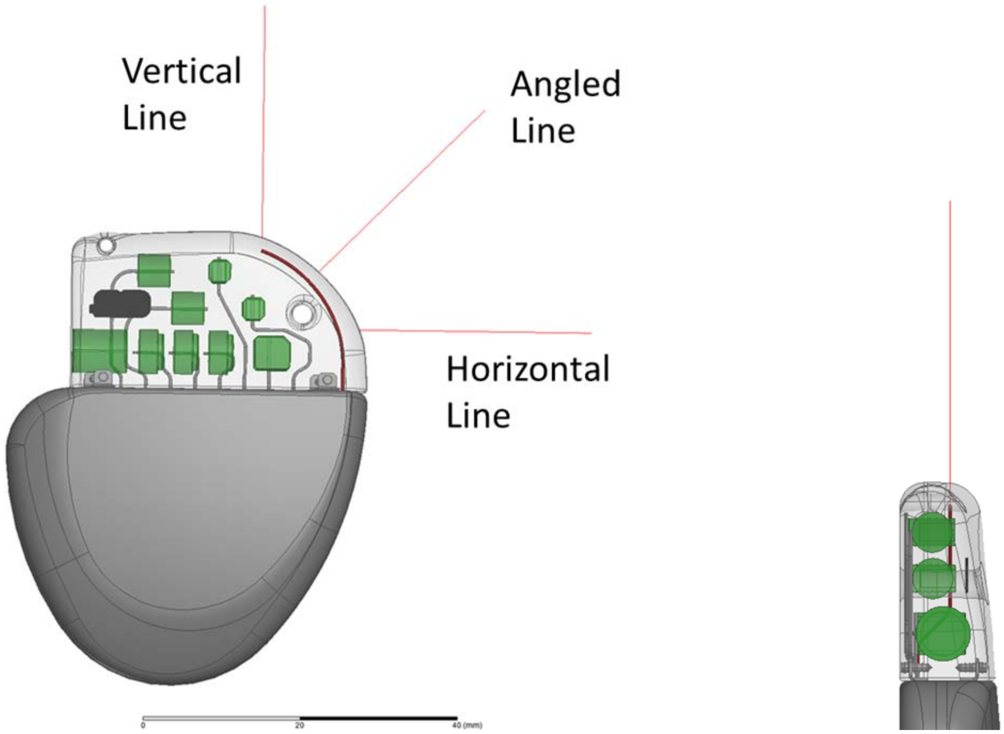

Figure 8: Location and orientation of E-field lines that start from the CRT-P Quad device surface

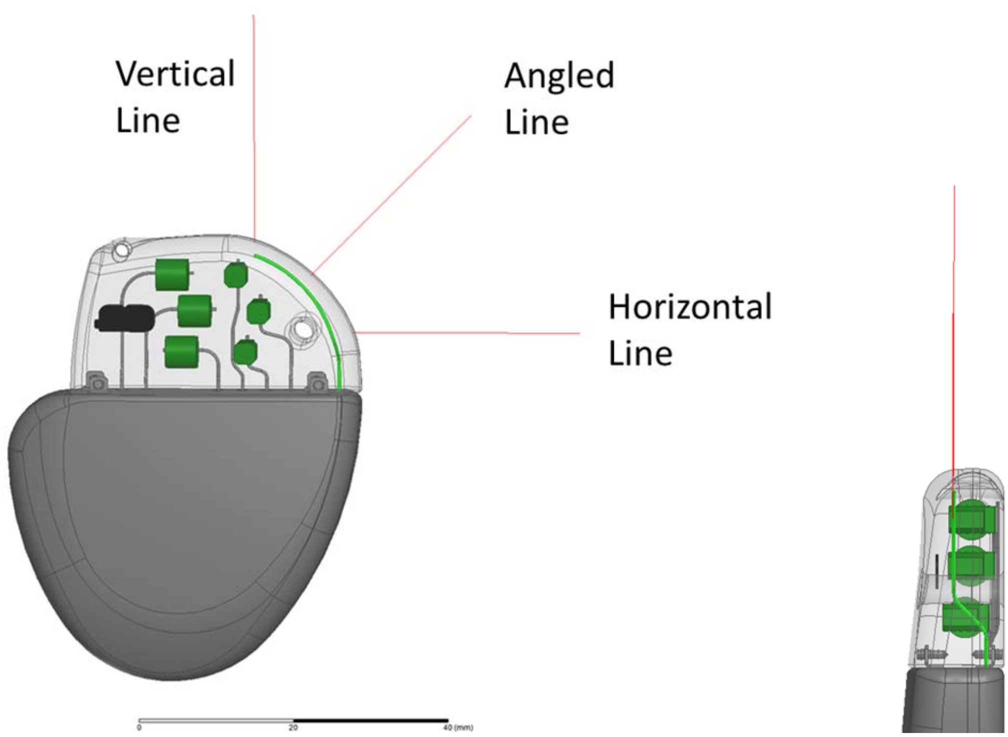

Figure 9: Location and orientation of E-field lines that start from the CRT-P BiPolar device surface

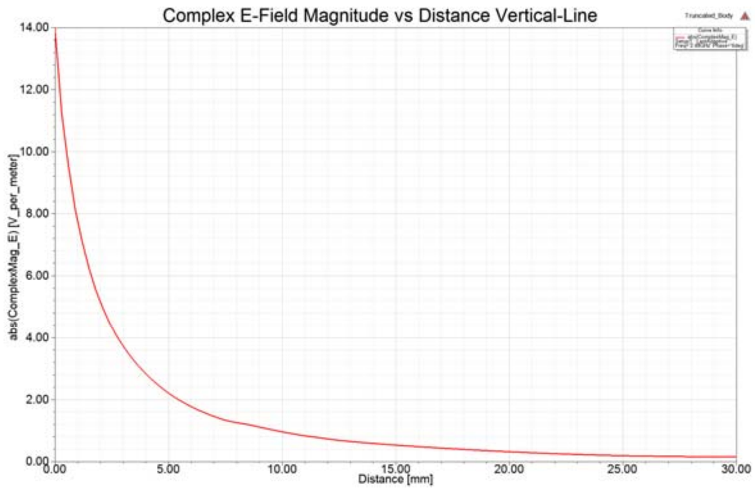

(a)

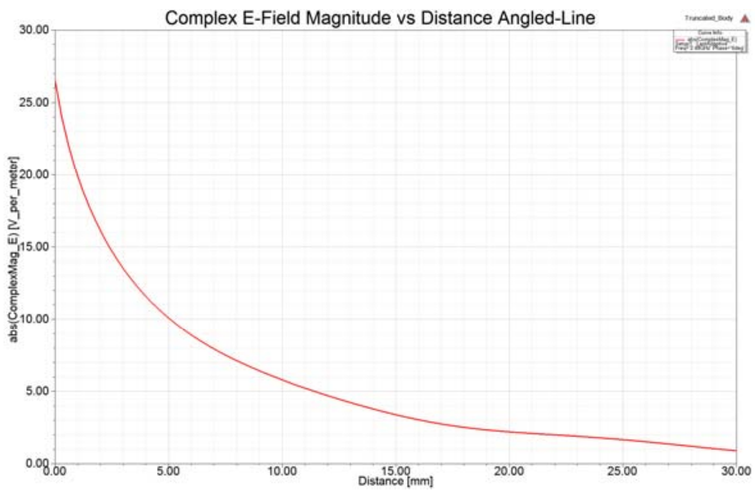

(b)

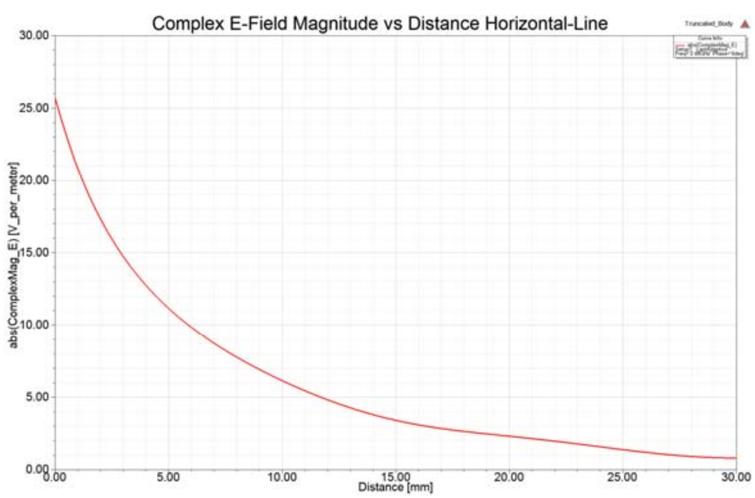

(c)

Figure 10: Simulated E-field strength versus distance from the CRT-P Quad device surface: (a) Vertical-Line (b) Angled-Line (c) Horizontal-Line

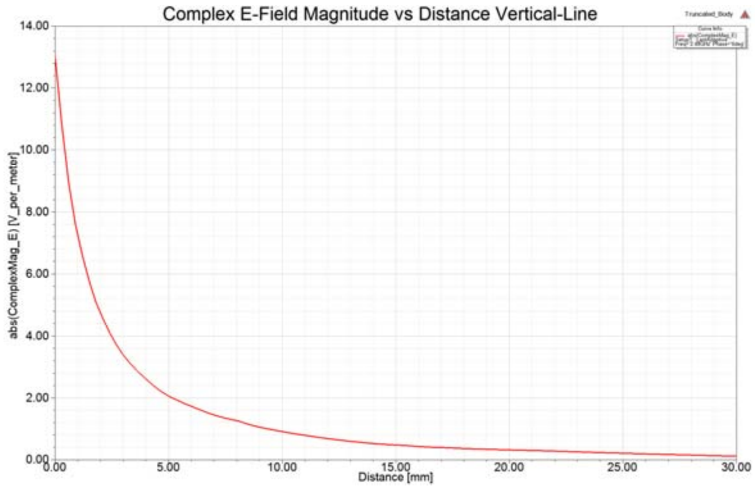

(a)

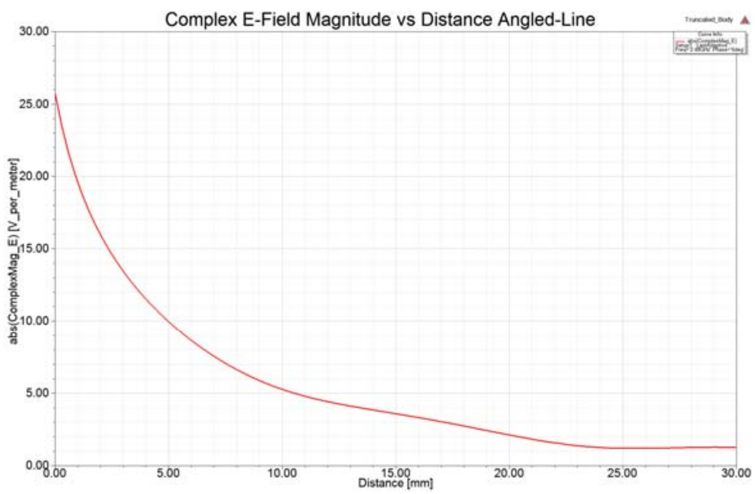

(b)

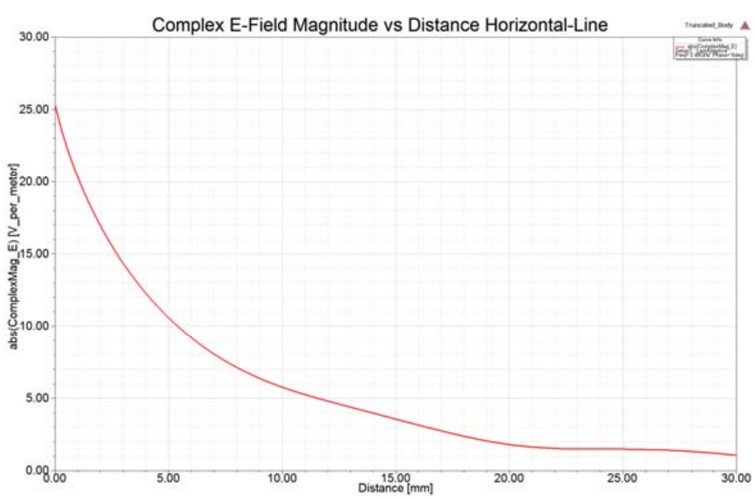

(c)

Figure 11: Simulated E-field strength versus distance from the CRT-P BiPolar device surface: (a) Vertical-Line (b) Angled-Line (c) Horizontal-Line

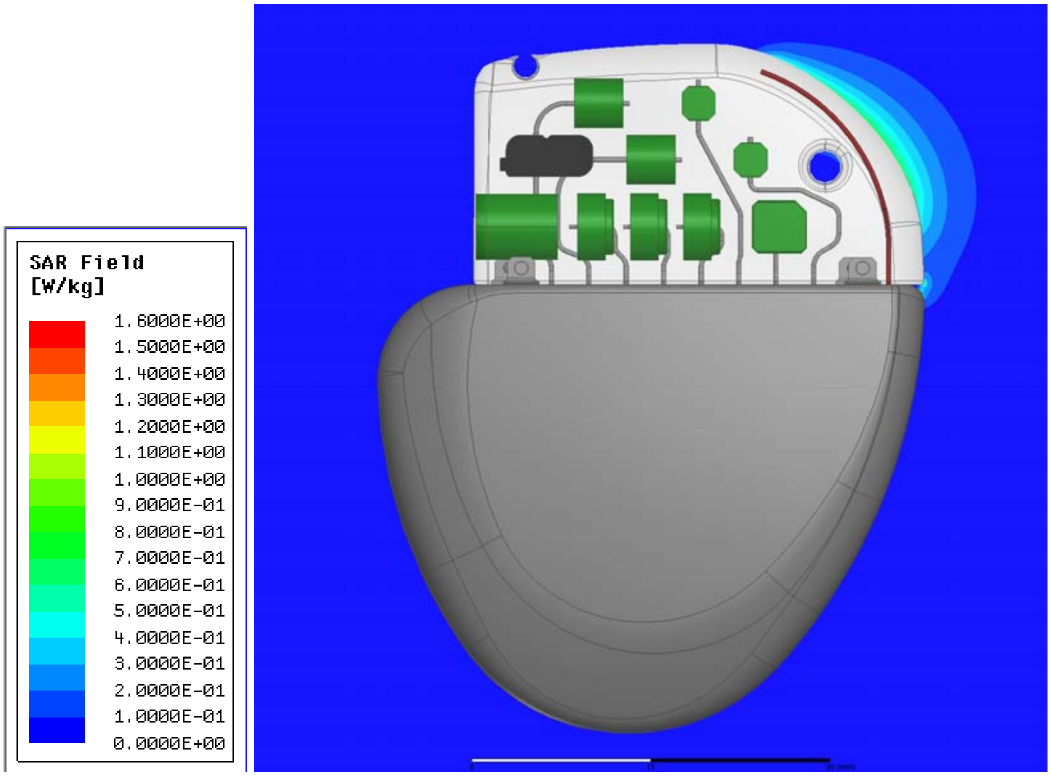

Figure 12: Zoom-In of HFSS simulated local SAR field in human body model cross-section with Implanted CRT-P Quad Device shown

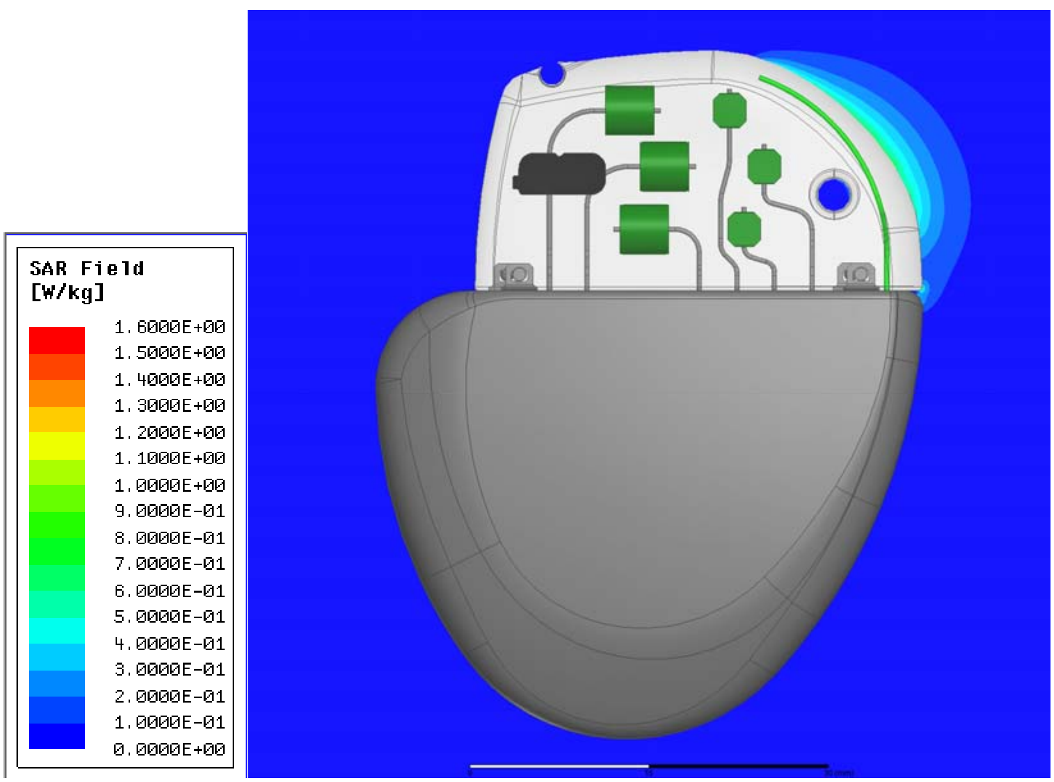

Figure 13: Zoom-In of HFSS simulated local SAR field in human body model cross-section with Implanted CRT-P BiPolar Device shown

The HFSS simulation result clearly shows that the peak electric field, i.e. the peak spatial SAR, is located in the tissue directly adjacent to the implanted RF antenna. This is illustrated in Figure 6 and 7 which shows the human torso model with the associated electric field strength due to the BTLE transmitter. The E-field strength versus distance from the device surface along EM wave propagation direction are plotted at two locations where peak E-field can be found based on Figure 6 and 7. Figure 8 and 9 shows the location and orientation of the E-field lines, and Figure 10 and 11 shows the dependence of the E-field strength versus the distance from device surface. It clearly shows that the E-field attenuates with the distance from the device. This also demonstrates the fact that for implanted devices, the peak 1-g average SAR should be determined by the tissue interface right adjacent to the device antenna in our model, but not sensitive to the device implant depth or location. Figure 12 and 13 are the simulated local SAR field plots for both CRT-P Quad and CRT-P BiPolar devices. It shows that the local SAR field is concentrated in a thin layer of interface tissue, and is below 1.6W/Kg in most area.

The spatial peak SAR averaged over any 1 gram (cube) of tissue was simulated with the human body torso model to be 0.1980 W/Kg for CRT-P Quad and 0.1915 W/kg for CRT-P BiPolar.

MODEL VALIDATION:

Ref [4] in attached appendix shows a report from Ansys Inc. about how HFSS complies with the accepted code validation and canonical benchmark problems prescribed in IEC 62704-1. In this attached report, to validate the accuracy of HFSS, SAR analysis simulations were run to mimic the measurement system performance check.

The above code validation and benchmarking results are based on earlier draft versions of the IEEE 1528.1 and IEC 62704-1 documents and ANSYS is currently working with the standards working group to establish procedures that are specific for finite element implementations. Due to the low SAR for these simulations, this preliminary code validation report from ANSYS should be sufficient for the two devices simulated for SAR.

The summary for the simulation results for HFSS as compared to results for FDTD are outlined in Table 4 below [4].

Freq. (MHZ)	% diff 1g average	% diff 10g average	% diff Feed Point	% diff 2cm offset
300	2.3%	1.5%	4.3%	1.9%
450	4.9%	0.3%	6.0%	2.2%
835	0.1%	0.2%	4.9%	0.2%
900	0.2%	0.4%	4.2%	0.4%
1450	0.4%	0.2%	7.0%	3.4%
1800	2.4%	1.8%	8.7%	2.5%
1900	0.6%	1.0%	6.9%	3.8%
2450	5.1%	3.6%	12.8%	0.6%
3000	0.4%	1.3%	9.4%	2.2%

Table 4: Percent difference between FDTD and HFSS simulation of SAR for a flat phantom

According to the benchmark results, the maximum difference on 1 g SAR between HFSS and FDTD at Bluetooth frequency is 5.1%. The SAR analysis shows that the CRT-P device 1 g peak SAR is 87.7% lower than the 1.6 W/Kg General Population/Uncontrolled exposure limit called out in §§2.1093. This margin (87.7%) below the exposure limit is approximately 16 times greater than the 5.1% deviation between FEA and FDTD results shown in above report. Therefore, we believe the quoted validation report from Ansys is sufficient to support our CRT-P SAR submission.

CONCLUSION:

The spatial peak SAR averaged over any 1 gram (cube) of tissue has been modeled / simulated to be 0.1980 W/Kg for CRT-P Quad and 0.1915 W/kg for CRT-P BiPolar. This is more than 9 dB below the 1.6 W/Kg General Population/Uncontrolled exposure limit called out in §§2.1093.

The Medtronic CRT-P family of Bluetooth Low Energy (BTLE) devices are therefore compliant with the FCC Rules (CFR 47, §§1.1307 and §§2.1093).

REFERENCES:

[1] Appendix: "Calculating the SAR", HFSS Technical Notes, Ansys Inc. (incorporated by permission)

[2] https://transition.fcc.gov/oet/rfsafety/dielectric.html

[3] IEEE TRANSACTIONS ON MAGNETICS, VOL. 36, NO. 4, JULY 2000

[4] Appendix: Ansys HFSS Compliance with IEEE / IEC 62704-1